STUDIES OF LOW-x PHYSICS AT THE LHCb*

Murilo Santana Rangel
on behalf of the LHCb Collaboration

Universidade Federal do Rio de Janeiro, Brazil

Received 16 December 2024, accepted 4 February 2025, published online 6 March 2025

The LHCb detector, with its unique forward rapidity coverage, is able to probe kinematic regions at Bjorken-x as low as 10^{-6}. This unique capability, combined with excellent momentum resolution, vertex reconstruction, and particle identification, enables precision measurements at low transverse momentum and forward rapidity. In this paper, we discuss the latest results of vector-meson exclusive production in pp and PbPb collisions and the production of light neutral mesons and D^0 mesons in lead–lead collisions, shedding light on partonic and nuclear dynamics at unprecedented small-x scales.

DOI:10.5506/APhysPolBSupp.18.1-A15

1. Introduction

These proceedings summarize the main results of five recent measurements of the LHCb Collaboration using data collected during Run 2 of the LHC [1–5]. The measurements cover a variety of physics phenomena, but they all share a common sensitivity to our understanding of the proton or nucleus structure, particularly in a region of longitudinal momentum fraction of partons that is considered low at LHC energies. The LHCb detector is a single-arm forward spectrometer covering the pseudorapidity range $2 < \eta < 5$, described in detail in Refs. [6] and [7]. Photons, electrons, and hadrons are identified by two Ring Imaging Cherenkov sub-detectors and a calorimeter system consisting of scintillating-pad (SPD) and preshower detectors, an electromagnetic calorimeter, and a hadronic calorimeter. Muons are identified by a system composed of alternating layers of iron and multiwire proportional chambers. The pseudorapidity coverage of the LHCb detector is extended by the HeRSCheL system, composed of forward shower counters at 114, 19.7, and 7.5 m upstream of the interaction point, and two

* Presented at the Diffraction and Low-x 2024 Workshop, Trabia, Palermo, Italy, 8–14 September, 2024.

downstream at 20 and 114 m [8]. The trigger consists of a hardware stage, based on information from the calorimeter and muon systems, followed by a software stage, which applies a full event reconstruction.

2. Charmonia production in ultra-peripheral PbPb collisions at the LHCb

In heavy-ion collisions, when two nuclei collide with an impact parameter larger than the sum of their radii, strong interactions are suppressed so that photon-induced interactions between the two ions dominate [9]. These collisions are called ultra-peripheral and they provide an excellent laboratory to study nuclear shadowing effects and the initial states of collisions with small x. In particular, the coherent photoproduction of J/ψ and $\psi(2S)$ mesons in ultra-peripheral collisions, when the photon couples coherently with the entire nucleus through the exchange of a Pomeron, is expected to probe the nuclear gluon distribution functions at a momentum transfer of about $m^2/4$, where m is the mass of the meson.

The LHCb Collaboration measured the coherent J/ψ and $\psi(2S)$ production reconstructed through the dimuon final state using the 2018 PbPb data sample collected at $\sqrt{s_{NN}} = 5.02$ TeV and corresponding to an integrated luminosity of $228 \pm 10\ \mu\mathrm{b}^{-1}$ [2]. The LHCb Collaboration also measured the ratio between the coherent $\psi(2S)$ and J/ψ production cross sections, where the uncertainties due to systematic effects and the luminosity determination largely cancel. This measurement can be used to constrain theoretical predictions and provide information on the choice of the meson wave function in dipole scattering models [10, 11] and the factorisation scale in perturbative Quantum Chromodynamics (QCD) models [12].

The measured differential cross sections for coherent J/ψ and $\psi(2S)$ photoproduction as functions of the meson rapidity in the PbPb centre-of-mass system (y^*) are shown in Fig. 1. The large parton distribution functions

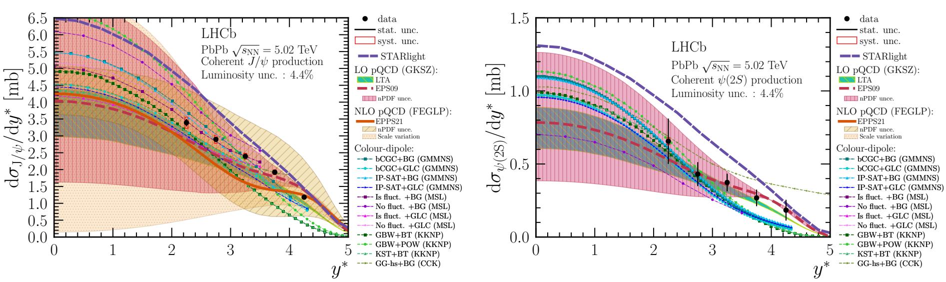

Fig. 1. Differential cross section as a function of the meson rapidity in the PbPb centre-of-mass system (y^*) for coherent (left) J/ψ and (right) $\psi(2S)$ photoproduction, compared to theoretical predictions.

(nPDF) uncertainties in Fig. 1 indicate that coherent charmonium photoproduction in heavy-ion collisions can be sensitive to the nuclear modification factors, especially to the modelling of the gluon shadowing, used in the LO pQCD calculations [12].

The differential cross sections as a function of meson transverse momentum are also measured separately for J/ψ and $\psi(2S)$ mesons in the ranges of $2.0 < y^{*} < 4.5$ [2]. The ratio of the cross sections between the coherent $\psi(2S)$ and J/ψ production, as a function of rapidity, is also determined for the first time in PbPb collisions and is found to be compatible with theoretical models.

3. Measurement of exclusive charmonia production

Central exclusive vector-meson production (CEP) in pp collisions is the quasi-elastic production of a single meson where the two initial-state protons remain intact. Exclusive charmonium production results from the conversion of a virtual photon into a $c\bar{c}$ pair, which hadronises into a J/ψ or $\psi(2S)$ meson. These processes probe the generalised parton distributions at the scale of the vector meson mass. The exclusivity of the process requires that, at leading order, two gluons are exchanged with the target hadron. Thus, the cross section approximately scales as gluon density squared [13–16]. Exclusive J/ψ and $\psi(2S)$ production in pp collisions at the LHC have previously been measured at centre-of-mass energies of $\sqrt{s} = 7$ TeV [17, 18] and 13 TeV [19].

The LHCb Collaboration measured the exclusive J/ψ and $\psi(2S)$ production in proton–proton collisions at $\sqrt{s} = 13$ TeV in the forward direction in ten intervals of rapidity between 2.0 and 4.5 [5]. The data used were collected with the LHCb detector at the LHC between 2016 and 2018, corresponding to an integrated luminosity of $4.4\,\mathrm{fb}^{-1}$, which is twenty times larger than that used in Ref. [19]. This larger sample permits a first measurement of the $\psi(2S)$ cross section in the same rapidity intervals as for the J/ψ cross section, and thus the determination of their ratio as a function of rapidity.

The resulting differential cross sections are shown in Fig. 2. Theoretical predictions are shown for comparison. While the J/ψ cross section agrees with the NLO prediction [20], which improves on the LO prediction [21], the $\psi(2S)$ cross section is significantly lower than both the LO and NLO predictions [22]. The J/ψ cross sections are used to determine the photoproduction cross section as a function of the photon–proton energy, which is reported in Ref. [5]. The results are consistent but more precise than those of Ref. [19]. The dependence of the J/ψ and $\psi(2S)$ cross sections on the total transverse momentum transfer is also determined in pp collisions for the first time and is found consistent with the behaviour observed at HERA [5].

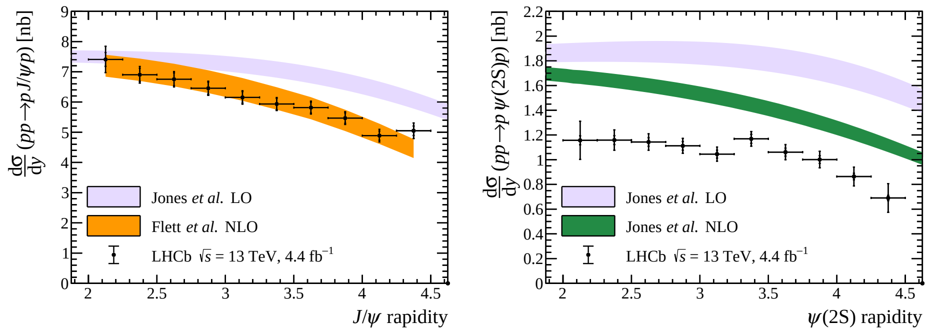

Fig. 2. Differential cross section for (left) J/ψ and (right) $\psi(2S)$ mesons. Theoretical predictions from Jones *et al.* [21, 22] and Flett *et al.* [20] are shown for comparison.

4. Observation of exotic $J/\psi\phi$ resonances in diffractive processes

The discovery of exotic QCD states has motivated an extensive theoretical and experimental effort to understand their properties [23]. The nature of exotic hadrons has been studied mainly in inclusive production or in exclusive beauty-hadron decays, in terms of properties such as mass, spin, and decay width. Resonant structures in the $J/\psi\phi$ mass spectrum have previously been observed in amplitude analyses of $B^+ \to J/\psi\phi K^+$ decays [24–26]. Five of those exotic candidates, $\chi_{c1}(4140)$, $\chi_{c1}(4274)$, and $\chi_{c1}(4685)$ with quantum numbers $J^{PC} = 1^{++}$ and $\chi_{c0}(4500)$ and $\chi_{c0}(4700)$ with $J^{PC} = 0^{++}$, can be produced in photon–photon or Pomeron–Pomeron processes, with the latter expected to dominate in pp collisions. Searches for the production of these exotic-hadron candidates in such processes can help elucidate their nature and distinguish between compact tetraquarks and molecular states [27–30].

The LHCb Collaboration measured the $J/\psi(\to \mu^+\mu^-)\phi(\to K^+K^-)$ production cross section for the first time in events with no additional detected activity, in which photon- and Pomeron-induced processes are expected to be dominant. An analysis of the $J/\psi\phi$ invariant-mass distribution is also performed and production cross sections are determined for each of the five resonant states and a nonresonant (NR) component. The data used correspond to an integrated luminosity of 5 fb^{-1} collected in pp collisions at $\sqrt{s} = 13$ TeV between 2016 and 2018 with the LHCb detector.

Events with additional activity, *i.e.*, with additional tracks reconstructed in the vertex detector (VELO tracks), are vetoed. The dimuon (dikaon) invariant mass is required to be in the range of $3036 < M_{\mu\mu} < 3156$ MeV ($1005 < M_{\rm KK} < 1035$ MeV). The $J/\psi\phi$ invariant mass is required to be less than 6000 MeV. After the selection requirements, 989 $J/\psi\phi$ candidates are retained.

Figure 3 shows the result of a maximum-likelihood fit performed on the resulting distribution using a model that consists of a sum of two exponential functions modified by the turn-on factor and convolved with the same resolution function. This distribution shows no clear mass structure, however when imposing the veto on additional VELO tracks, a resonant structure appears, which indicates the presence of a photon-induced or Pomeron-induced mechanism. The $J/\psi\phi$ invariant-mass spectrum is described by a model consisting of five resonances, namely $\chi_{c1}(4140)$, $\chi_{c1}(4274)$, $\chi_{c0}(4500)$, $\chi_{c1}(4685)$, and $\chi_{c0}(4700)$, and a nonresonant component. The resonances considered are the ones observed in Refs. [24–26] with quantum numbers compatible with diffractive photon-induced or Pomeron-induced production processes. The resulting $J/\psi\phi$ invariant-mass distribution for signal candidates is shown in Fig. 3 overlaid with the results of an extended maximum-likelihood fit of the signal model.

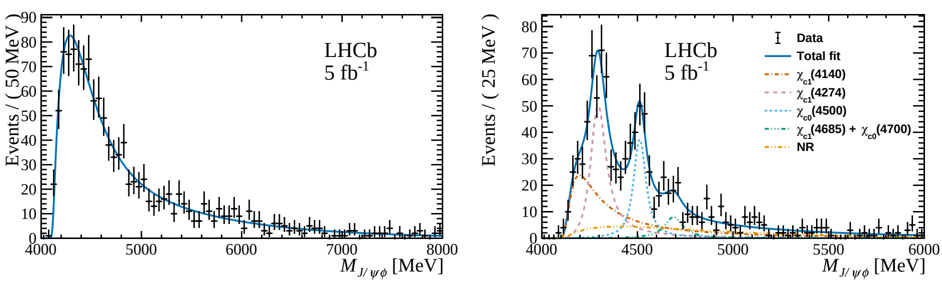

Fig. 3. Left: Invariant-mass distribution of $J/\psi\phi$ candidates for the sideband sample composed of events with more than four reconstructed VELO tracks. Note that all other selection requirements are applied, including the J/ψ and ϕ mass-window requirements. Right: Invariant-mass distribution of $J/\psi(\to \mu^+\mu^-)\phi(\to K^+K^-)$ candidates in the signal sample after selection. The fit components are shown as dashed lines.

Several clear resonant structures are observed in the invariant-mass distribution of these $J/\psi\phi$ candidates, which is well described by a model containing five resonant and one nonresonant components. This is the first observation of $J/\psi\phi$ production in diffractive processes and therefore helps determine the underlying nature of exotic states.

5. Prompt D^0 nulcear modification factor in pPb collisions

Charm and beauty quarks are produced in the early stage of ultra-relativistic heavy-ion collisions and are strongly affected by the presence of deconfined hot nuclear matter, known as quark–gluon plasma (QGP) [31], as well as by cold nuclear matter (CNM) effects. At LHC energies, the most relevant effect is from the initial state, where the parton distribution functions in a nuclear environment (nPDF) [32–34] differ from those in isolated nucleons at all values of Bjorken momentum fraction x.

Recent measurements have led to significantly reduced uncertainties of nPDFs in the small-x region [35, 36], which motivates measurements of the nuclear modification factor $R_{p\mathrm{Pb}}$ of prompt D^0 mesons in pPb collisions at $\sqrt{s_{NN}} = 8.16$ TeV. The quantity $R_{p\mathrm{Pb}}$ is defined as the ratio of the cross section in pPb collisions to the corresponding cross section in pp collisions scaled by the mass number of Pb. This measurement uses a data sample 20 times larger than that used for the LHCb D^0 measurements at $\sqrt{s_{NN}} = 5.02$ TeV [37].

The nuclear modification factor of the D^0 meson as a function of p_{T} is shown in Fig. 4, where eight panels report the results in different y^* intervals of $\Delta y^* = 0.5$ and the two left panels are in the common range between the forward and backward rapidity coverage, $2.5 < |y^*| < 4$. A significant suppression of the cross section in pPb collisions, with respect to that in pp collisions scaled by the lead mass number, is observed at forward rapidity as well as at backward rapidity up to $y^* \sim -3.5$.

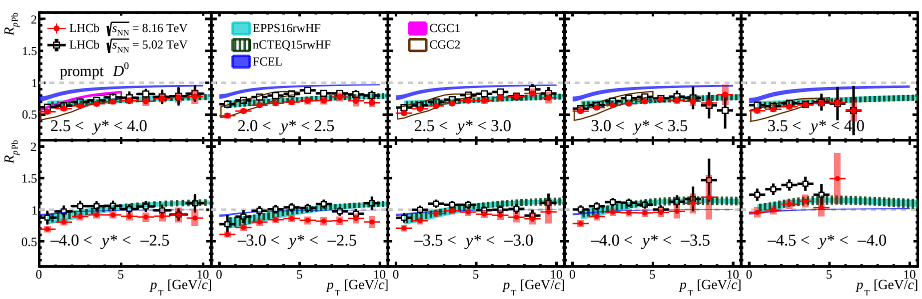

Fig. 4. Nuclear modification factor as a function of p_{T} in different y^* intervals for prompt D^0 mesons in the (top) forward and (bottom) backward regions. The error bars show the statistical uncertainties and the boxes show the systematic uncertainties. The LHCb results at $\sqrt{s_{NN}} = 5.02$ TeV [37] and theoretical calculations at $\sqrt{s_{NN}} = 8.16$ TeV from Refs. [38–42] are also shown. For LHCb results at $\sqrt{s_{NN}} = 5.02$ TeV, the error bars show the quadric sum of statistical and systematic uncertainties.

The nuclear modification factors are measured with high accuracy and show strong CNM. A stronger suppression than the predictions of nPDF calculations is observed for the lowest transverse momentum region of $p_{\mathrm{T}} < 1$ GeV at forward rapidity. For the backward rapidity range of $-3.5 < y^* < -2.5$, the $R_{p\mathrm{Pb}}$ values are lower than nPDF calculations at $p_{\mathrm{T}} > 6$ GeV with a significance of 2.0–3.8 standard deviations, indicating a weaker antishadowing effect than the model or additional final-state effects at backward rapidity. This is the most precise measurement of the prompt D^0 production in pPb collisions to date, providing unique constraints to improve nPDF parameterization down to $x \sim 10^{-5}$.

6. Studies of η and η' production in pp and pPb collisions

Studying the production of π^0, η, and η' mesons in heavy-ion collisions allows for the isolation of the mass and isospin dependence of nuclear effects, which can help reveal the origin of QGP-like phenomena in small-collision systems. The collective radial flow of the QGP, for example, is expected to produce larger enhancements for heavier particles, as heavier particles must receive a larger momentum boost in order to comove with an expanding medium [43, 44]. The production of η mesons has been studied extensively in small-collision systems at central rapidity at RHIC and the LHC [45–53]. However, there are no studies of η meson production at forward or backward rapidity in collisions involving heavy ions. Studying both η and η' production at forward and backward rapidities helps reveal the mass and rapidity dependence of nuclear effects in heavy-ion collisions.

The η and η' cross sections are measured differentially in p_{T} in pp collisions at $\sqrt{s} = 5.02$ and 13 TeV, and in pPb collisions at 8.16 TeV. The η-meson cross sections are combined with the previous LHCb measurements of the π^0 differential cross sections to calculate the η/π^0 cross-section ratio. The measurements are performed in the center-of-mass rapidity (y_{cm}) ranges $2.5 < y_{\mathrm{cm}} < 3.5$ and $-4.0 < y_{\mathrm{cm}} < -3.0$, which correspond to the overlapping portions of the pp and pPb fiducial regions. The center-of-mass rapidity is related to the lab-frame rapidity y_{lab} by $y_{\mathrm{cm}} = y_{\mathrm{lab}} - 0.465$ in pPb collisions and $|y_{\mathrm{cm}}| = y_{\mathrm{lab}}$ in pp collisions.

The differential cross sections are used to calculate nuclear modification factors, which are shown in Fig. 5. In the forward region, the η, π^0, and η' results all agree where their fiducial regions overlap. The observed suppression is consistent with the effects of nuclear shadowing of the gluon density seen in global nPDF analyses [32, 36, 54]. In the backward region, the π^0 and η measurements deviate at low p_{T} and converge for $p_{\mathrm{T}} > 3$ GeV. In this region, the π^0, η, and η' measurements all agree. The results show no significant evidence for mass dependence of the nuclear modification factor of light-neutral mesons.

This is the first study of η-meson production at forward and backward rapidity at the LHC and the first study of η'-meson production in high-energy proton–ion collisions. The measured differential cross sections are compared to predictions from PYTHIA 8 and EPOS4 and neither event generator successfully describes the measurements for every data set and rapidity region [3]. The measured nuclear modification factors of the π^0, η, and

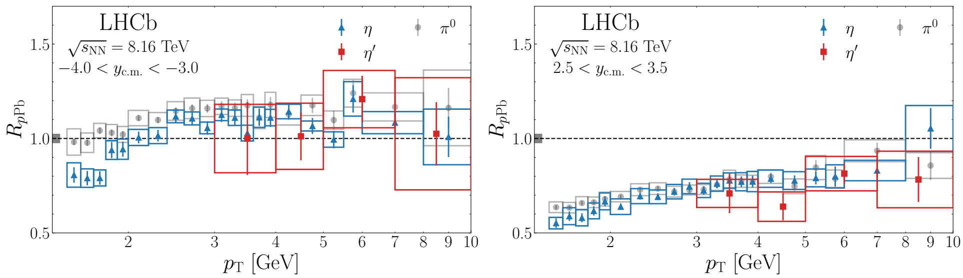

Fig. 5. Measured η and η' nuclear modification factors in the (left) backward and (right) forward regions. Error bars show the statistical uncertainties, while the boxes show the systematic uncertainties except for the uncertainty associated with the luminosity, which is fully correlated between measurements. The luminosity uncertainty is shown as a dark gray shaded box. The η and η' results are compared to the π^0 data from Ref. [55].

η' mesons all agree at both forward and backward rapidity for $p_{\rm T} > 3$ GeV. These measurements provide important information for the interpretation of baryon and strangeness enhancement studies in small collision systems.

7. Conclusions

This contribution highlights five LHCb results sensitive to low x, including the observation of exotic states in diffractive events. We demonstrate that these measurements can constrain and improve phenomenological models, with future studies anticipated to further enrich this understanding.

M.S.R. was partially supported by CNPq, FAPERJ, and INCT-CERN (process No. 406672/2022-9).

REFERENCES

[1] LHCb Collaboration (R. Aaij *et al.*), *Phys. Rev. Lett.* **131**, 102301 (2023), arXiv:2205.03936 [hep-ex].

[2] LHCb Collaboration (R. Aaij *et al.*), *J. High Energy Phys.* **2023**, 146 (2023), arXiv:2206.08221 [hep-ex].

[3] LHCb Collaboration (R. Aaij *et al.*), *Phys. Rev. C* **109**, 024907 (2024), arXiv:2310.17326 [hep-ex].

[4] LHCb Collaboration (R. Aaij *et al.*), arXiv:2407.14301 [hep-ex].

[5] LHCb Collaboration (R. Aaij *et al.*), arXiv:2409.03496 [hep-ex].

[6] LHCb Collaboration (A.A. Alves Jr. *et al.*), *J. Instrum.* **3**, S08005 (2008).

[7] LHCb Collaboration (R. Aaij *et al.*), *Int. J. Mod. Phys. A* **30**, 1530022 (2015), arXiv:1412.6352 [hep-ex].

[8] K. Carvalho Akiba *et al.*, *J. Instrum.* **13**, P04017 (2018), arXiv:1801.04281 [physics.ins-det].

[9] C.A. Bertulani, S.R. Klein, J. Nystrand, *Annu. Rev. Nucl. Part. Sci.* **55**, 271 (2005), arXiv:nucl-ex/0502005.
[10] H. Kowalski, L. Motyka, G. Watt, *Phys. Rev. D* **74**, 074016 (2006), arXiv:hep-ph/0606272.
[11] V.P. Gonçalves, M.V.T. Machado, *Phys. Rev. C* **84**, 011902 (2011), arXiv:1106.3036 [hep-ph].
[12] V. Guzey, E. Kryshen, M. Zhalov, *Phys. Rev. C* **93**, 055206 (2016), arXiv:1602.01456 [nucl-th]
[13] M.G. Ryskin, *Z. Phys. C* **57**, 89 (1993).
[14] H. Mäntysaari, J. Penttala, *J. High Energy Phys.* **2022**, 08 (2022), arXiv:2204.14031 [hep-ph].
[15] C.A. Flett *et al.*, *Phys. Rev. D* **101**, 094011 (2020), arXiv:1908.08398 [hep-ph].
[16] M. Diehl, *Phys. Rep.* **388**, 41 (2003), arXiv:hep-ph/0307382.
[17] LHCb Collaboration (R. Aaij *et al.*), *J. Phys. G: Nucl. Part. Phys.* **40**, 045001 (2013), arXiv:1301.7084 [hep-ex].
[18] LHCb Collaboration (R. Aaij *et al.*), *J. Phys. G: Nucl. Part. Phys.* **41**, 055002 (2014), arXiv:1401.3288 [hep-ex].
[19] LHCb Collaboration (R. Aaij *et al.*), *J. High Energy Phys.* **2018**, 167 (2018), arXiv:1806.04079 [hep-ex].
[20] C.A. Flett, A.D. Martin, M.G. Ryskin, T. Teubner, *Phys. Rev. D* **102**, 114021 (2020), arXiv:2006.13857 [hep-ph].
[21] S.P. Jones, A.D. Martin, M.G. Ryskin, T. Teubner, *J. High Energy Phys.* **2013**, 085 (2013), arXiv:1307.7099 [hep-ph].
[22] S.P. Jones, A.D. Martin, M.G. Ryskin, T. Teubner, *J. Phys. G: Nucl. Part. Phys.* **41**, 055009 (2014), arXiv:1312.6795 [hep-ph].
[23] N. Brambilla *et al.*, *Phys. Rep.* **873**, 1 (2020).
[24] LHCb Collaboration (R. Aaij *et al.*), *Phys. Rev. Lett.* **118**, 022003 (2017), arXiv:1606.07895 [hep-ex].
[25] LHCb Collaboration (R. Aaij *et al.*), *Phys. Rev. D* **95**, 012002 (2017), arXiv:1606.07898 [hep-ex].
[26] LHCb Collaboration (R. Aaij *et al.*), *Phys. Rev. Lett.* **127**, 082001 (2021), arXiv:2103.01803 [hep-ex].
[27] S.J. Brodsky, R.F. Lebed, *Phys. Rev. D* **91**, 114025 (2015).
[28] A. Cerri *et al.*, *CERN Yellow Rep.: Monogr.* **7**, 867 (2019), arXiv:1812.07638 [hep-ph].
[29] A. Esposito, C.A. Manzari, A. Pilloni, A.D. Polosa, *Phys. Rev. D* **104**, 114029 (2021).
[30] A. Esposito, F. Piccinini, A. Pilloni, A.D. Polosa, *J. Mod. Phys.* **4**, 1569 (2013).
[31] K. Yagi, T. Hatsuda, Y. Miake, «Quark–Qluon Plasma: From Big Bang to Little Bang», 2005.
[32] K.J. Eskola, P. Paakkinen, H. Paukkunen, C.A. Salgado, *Eur. Phys. J. C* **82**, 413 (2022), arXiv:2112.12462 [hep-ph].

[33] D. de Florian, R. Sassot, *Phys. Rev. D* **69**, 074028 (2004), arXiv:hep-ph/0311227.
[34] M. Hirai, S. Kumano, T.-H. Nagai, *Phys. Rev. C* **76**, 065207 (2007), arXiv:0709.3038 [hep-ph].
[35] K.J. Eskola, I. Helenius, P. Paakkinen, H. Paukkunen, *J. High Energy Phys.* **2020**, 037 (2020), arXiv:1906.02512 [hep-ph].
[36] R. Abdul Khalek *et al.*, *Eur. Phys. J. C* **82**, 507 (2022), arXiv:2201.12363 [hep-ph].
[37] LHCb Collaboration (R. Aaij *et al.*), *J. High Energy Phys.* **2017**, 090 (2017), arXiv:1707.02750 [hep-ex].
[38] K.J. Eskola, P. Paakkinen, H. Paukkunen, C.A. Salgado, *Eur. Phys. J. C* **77**, 163 (2017), arXiv:1612.05741 [hep-ph].
[39] K. Kovarik *et al.*, *Phys. Rev. D* **93**, 085037 (2016), arXiv:1509.00792 [hep-ph].
[40] B. Ducloué, T. Lappi, H. Mäntysaari, *Nucl. Part. Phys. Proc.* **289–290**, 309 (2017), arXiv:1612.04585 [hep-ph].
[41] Y.-Q. Ma, P. Tribedy, R. Venugopalan, K. Watanabe, *Phys. Rev. D* **98**, 074025 (2018), arXiv:1803.11093 [hep-ph].
[42] F. Arleo, François, G. Greg, S. Peigné, *J. High Energy Phys.* **2022**, 164 (2022), arXiv:2107.05871 [hep-ph].
[43] A.M. Sickles, *Phys. Lett. B* **731**, 51 (2014), arXiv:1309.6924 [nucl-th].
[44] A. Ayala, E. Cuautle, J. Magnin, L.M. Montano, *Phys. Rev. C* **74**, 064903 (2006), arXiv:nucl-th/0603039.
[45] PHENIX Collaboration (A. Adare *et al.*), *Phys. Rev. D* **83**, 052004 (2011), arXiv:1005.3674 [hep-ex].
[46] PHENIX Collaboration (A. Adare *et al.*), *Phys. Rev. D* **83**, 032001 (2011), arXiv:1009.6224 [hep-ex].
[47] ALICE Collaboration (B. Abelev *et al.*), *Phys. Lett. B* **717**, 162 (2012), arXiv:1205.5724 [hep-ex].
[48] ALICE Collaboration (S. Acharya *et al.*), *Eur. Phys. J. C* **78**, 263 (2018), arXiv:1708.08745 [hep-ex].
[49] ALICE Collaboration (S. Acharya *et al.*), *Eur. Phys. J. C* **78**, 624 (2018), arXiv:1801.07051 [nucl-ex].
[50] ALICE Collaboration (S. Acharya *et al.*), *Phys. Lett. B* **827**, 136943 (2022), arXiv:2104.03116 [nucl-ex].
[51] STAR Collaboration (B.I. Abelev *et al.*), *Phys. Rev. C* **81**, 064904 (2010), arXiv:0912.3838 [hep-ex].
[52] STAR Collaboration (L. Adamczyk *et al.*), *Phys. Rev. D* **86**, 051101 (2012), arXiv:1205.6826 [nucl-ex].
[53] PHENIX Collaboration (A. Adare *et al.*), *Phys. Rev. D* **90**, 072008 (2014), arXiv:1406.3541 [hep-ex].
[54] N. Armesto, *J. Phys. G: Nucl. Part. Phys.* **32**, R367 (2006).
[55] LHCb Collaboration (R. Aaij *et al.*), *Phys. Rev. Lett.* **131**, 042302 (2023), arXiv:2204.10608 [hep-ex].